remote sensing

MDPI

Article

Geomorphological Mapping and Erosion of Abandoned Tailings in the Hiendelaencina Mining District (Spain) from Aerial Imagery and LiDAR Data

Silvia Martín-Velázquez [1,2,*], Inmaculada Rodríguez-Santalla [1,2], Nikoletta Ropero-Szymańska [1], David Gomez-Ortiz [1,2], Tomás Martín-Crespo [1,2] and Cristina de Ignacio-San José [3]

[1] Departamento de Biología, Geología, Física y Química Inorgánica, Escuela Superior de Ciencias Experimentales y Tecnología, Universidad Rey Juan Carlos, C/Tulipán s/n, 28933 Móstoles, Madrid, Spain
[2] Research Group in Environmental Geophysics and Geochemistry, Universidad Rey Juan Carlos, C/Tulipán s/n, 28933 Móstoles, Madrid, Spain
[3] Departamento de Mineralogía y Petrología, Facultad de Ciencias Geológicas, Universidad Complutense de Madrid, C/José Antonio Novais, 12, 28040 Madrid, Madrid, Spain
* Correspondence: silvia.martin@urjc.es

Abstract: The Hiendelaencina district in Spain was the most important silver producer in Europe during 1844–1925. At the end of the 20th century, with mines having closed, some waste rock dumps were reprocessed, and the sludge from the flotation process was stored in two tailings ponds. When this activity ceased, the residues began to be eroded and disperse. In this study, the state of degradation of both deposits was evaluated using historical mapping and light detection and ranging (LiDAR) data, incorporated into a Geographic Information System. In the aerial images (1946–2018), mine tailings and their main erosive and sedimentary forms were mapped. Geoforms linked to hydrological (channels, gullies, alluvial cones), wind (eolian mantles), hydric–gravitational (colluvium) and anthropic (motorbike tracks) processes which move sludge into the surrounding areas were identified. A net loss of 8849 m^3 of sludge, a release of 10.3 t of potentially polluting substances and a high erosion rate of 346 t/ha*year were calculated based on LiDAR data from 2009 and 2014. The ponds show a current high degree of erosion that could increase due to both human activity and the growing frequency of drought and torrential rain periods if stabilization measures are not undertaken.

Keywords: mine tailings; mining geomorphology; water erosion; eolian erosion; anthropic erosion; erosion rate; aerial imagery; LiDAR data

check for updates

Citation: Martín-Velázquez, S.; Rodríguez-Santalla, I.; Ropero-Szymańska, N.; Gomez-Ortiz, D.; Martín-Crespo, T.; de Ignacio-San José, C. Geomorphological Mapping and Erosion of Abandoned Tailings in the Hiendelaencina Mining District (Spain) from Aerial Imagery and LiDAR Data. *Remote Sens.* **2022**, *14*, 4617. https://doi.org/10.3390/rs14184617

Academic Editor: Alberto Refice

Received: 11 July 2022
Accepted: 13 September 2022
Published: 15 September 2022

Publisher's Note: MDPI stays neutral with regard to jurisdictional claims in published maps and institutional affiliations.

Copyright: © 2022 by the authors. Licensee MDPI, Basel, Switzerland. This article is an open access article distributed under the terms and conditions of the Creative Commons Attribution (CC BY) license (https://creativecommons.org/licenses/by/4.0/).

1. Introduction

Spain was one of the main producers of metals during the 19th century, and the ceasing of mining activity led to the abandonment of numerous slagheaps, such as waste rock dumps and mining ponds, throughout the 20th century [1,2]. Mining sludge is a mixture of crushed rock, solid residues from the extraction and treatment of the material, washing liquid, and heavy metals resulting from metallurgical flotation processing, and has a medium-to-fine grain size. When the ponds are abandoned, the sludge dries up and is weathered and eroded by water and wind. The mobilization of metals causes a serious environmental impact, especially in the surrounding areas [3–8].

Weather conditions are a determinant in the dispersion of pollutants both by water and by wind [3,5,7,9]. Regarding water erosion, torrential rains have great erosive force and can create steep escarpments and deep gullies in the ponds. Wind erosion is significant in regions with a Mediterranean climate characterized by low humidity, which translates into low cohesion of the sludge and the scarce development of vegetation cover. In this context, the airborne transport of the finer fractions of sludge can affect soil, water, and wildlife.

Surface erosion processes take place on the mining ponds until they reach a stable geomorphology adapted to the environmental conditions [10,11]. To evaluate the impact of these deposits, it is important to determine their present degree of erosion and the associated hazard [12]. Remote sensing techniques combined with field surveys are commonly used for monitoring terrain changes and estimating erosion rates at different temporal and spatial scales [13–17]. Total station and GNSS surveys, terrestrial and airborne light detection and ranging (LiDAR), or structure from motion (SfM) and multi-view stereo (MVS) photogrammetric methods, among others, allow the acquisition of altitude data to generate digital terrain models (DTM). Additionally, when large temporal coverage is required, aerial photographs or historical maps are analyzed to detect and measure landscape changes [13]. These techniques and documents are also used in mining sites to quantify the amount of mining waste moved and the rate at which it is eroded, identify eroded areas, and even establish potential areas of contamination [10,12,18–20]. On the other hand, some works focus on the prediction of soil erosion in mine areas by applying the revised universal soil loss equation (RUSLE) [21,22]. However, there is a scarcity of studies that calculate volumes and tonnages of mining waste stored and/or moved from sludge ponds [10,23,24].

At the turn of the 19th and 20th century, the town of Hiendelaencina in Spain was one of the leading silver producers in Europe [25–28]. Mining ceased due to both progressively falling ore prices and the depletion of the better productive mines, but at the end of the 20th century it resumed with the re-processing of waste rock dumps. The sludge resulting from the flotation process was collected in two ponds registered within the National Inventory of Sludge Deposits [29]. These deposits have been abandoned for three decades, and erosion and transport processes have been moving the sludge both in and around their boundaries. In dry periods, salt crusts form and the wind erodes the finest particles, generating dust clouds that reach the nearby Hiendelaencina town (Figure 1). On the other hand, the ponds are not watertight, and leachates could potentially leak into the underlying soil on which they were deposited. For these reasons, the environmental impact of these mining deposits is considered as high [29].

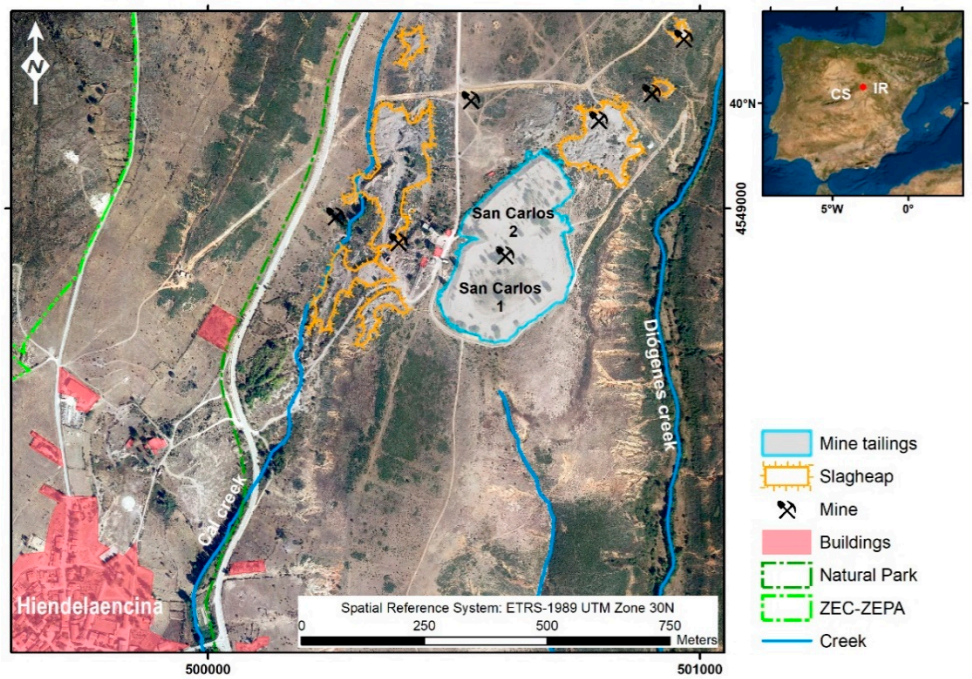

Figure 1. Location of the sludge ponds and other elements of the San Carlos mine on the orthophoto of the 2018 flight (Vector data source [30,31]). ZEC-ZEPA, Zone of Special Conservation–Zone of Special Bird Protection. The red circle in the regional map locates the study area. CS, Central System. IR, Iberian Range.

Over recent decades, several studies have been carried out in the mining district of Hiendelaencina on mineralization, mining, mining heritage, and tourist use [26–28,32–34], but none on physicochemical state, stability, or the extent to which the abandoned mine ponds are affecting the area. Reclamation techniques have not been implemented in the area to reduce erosion and, in order to evaluate the possible effects on the environment, it is essential to characterize these deposits as a first step. Therefore, the aim of this study is to estimate the state of erosion of the Hiendelaencina ponds by mapping the main geomorphological features and their evolution over time, and estimate the rate of erosion and the release of potentially hazardous elements into the surrounding areas. Although the use of unmanned aerial vehicles (UAVs) and terrestrial images is providing high-spatial-resolution 3D models [14,15,17,20], abundant aerial imagery and aerial LiDAR data are available, free of charge, for the study area. Thus, geomorphological mapping was conducted from the 2018 orthophoto and field observations. The areal evolution of the ponds was carried out based on aerial images from 1946 to 2018. The erosion rate was calculated from the volume of sludge obtained from the LiDAR data from 2009 and 2014. The amounts of potentially hazardous elements released were calculated from various physicochemical parameters of the sludge from Hiendelaencina and other mining areas. The Geographic Information System (GIS) software ArcGIS was used to manage and analyze aerial imagery and aerial LiDAR data.

2. Materials and Methods

2.1. Study Area

The Hiendelaencina mining district was the most important European silver-producing area between 1844 and 1925 [25–28]. In 1844, thirteen silver veins were discovered and, in the most productive one of them, twelve mines started to operate. Although the origin of the ore was the result of various orogenic processes, silver was deposited mainly in quartz-rich vertical fractures that crossed a Paleozoic gneiss and quartzite basement, which were reactivated during the Alpine orogeny. In the gneisses, acanthite (Ag_2S), stephanite (Ag_5SbS_4), and kerargyrite (ClAg) were intergrown with barite ($BaSO_4$) and galena (PbS). The American or European amalgamation method was used to extract the silver from the ore, and the wastes were deposited in dumps near the mines. After a succession of prosperous and declining periods, mining came to a standstill in 1925.

Between 1980 and 1990, mining was resumed with the processing of materials from waste rock dumps [26–28]. The flotation process was carried out in the vicinity of the old San Carlos mine, 1 km north–east of the town of Hiendelaencina. The resulting sludge was deposited in two ponds, with upstream recharge, on a bedrock of tertiary gravel and clay discordant over the gneisses. Although the ponds are currently abandoned, they have an active drainage system that allows them to achieve high compaction and mechanical stability. The estimated volume of sludge is 300,000 m^3 in the north pond (San Carlos 2) and 330,000 m^3 in the south pond (San Carlos 1) (Figure 1) [29].

Regarding the main geographical features, this region is in the area where the mountain belts of the Central System and the Iberian Range meet. The ponds are specifically located on a foothill with scrubland vegetation at an average altitude of 1085 m, with uniform, less than 15% gradient slopes. The foothills are bordered by the Diógenes and Cal creeks, which are tributaries of the Bornova river which is dammed in this area for water supply and irrigation (Figure 1). To the west of the ponds, and within the municipality of Hiendelaencina, the Sierra Norte de Guadalajara Natural Park and the ZEC–ZEPA (Zone of Special Conservation–Zone of Special Bird Protection) zone of the Sierra de Ayllón can be found, owing to the significant geodiversity, landscape and botanical value of the mountains [35]. The climate is a warm-summer Mediterranean type according to the Köppen classification (Csb) [36]. The average annual rainfall is around 600 mm, with average annual maximum daily rainfall in May and October (46 mm/day on average) and lows in August. The average annual temperature is 12.5 °C, with maximum temperatures in July and August and minimum temperatures in December and January. The average wind

speed is 14.2 km/h, with maximum gusts of 127 km/h [37]. The windiest periods are between October and May. Winds from the north and west prevail, although in dry periods they come from the west, east and south [38].

2.2. Time Evolution and Geomorphological Mapping of Mine Tailings

The time evolution and geomorphological mapping of the ponds were carried out by analyzing the aerial images available from the National Geographic Information Center of the Spanish National Geographic Institute (IGN) [30]. Data were collected from 1946 to 2018, with flight scales from 1:43,200 to 1:20,000 and pixel sizes from 0.27 to 1 m (Table 1). The 1973–1986, 1980–1986 and 2002 (quinquennial flight of IGN) flights were georeferenced with mean residual errors of 0.32, 0.57 and 0.48 m, respectively. The rest of the data were already georeferenced by IGN with RMSE x,y $\leq$ 1.00 m [30].

Table 1. Characteristics of the aerial imagery used in the study. AMS, American Army Map Service; OLISTAT, Olive Statistics; PNOA, National Aerial Orthophotography Plan; SIGPAC, Geographic Information System of Agricultural Parcels. Time span or years in the Flight Name column indicate when the photogrammetric flights were performed over the whole or part of the Spanish territory. Dates in the Frame Date column indicate when the aerial images were taken in the study area (these data are not specified in the Interministerial flight).

Flight Name	Frame Date	Scale	Pixel Size (GSD; m)	Original Frame Format
AMS 1945–1946. Ministry of Defense	20 July 1946	1:43,200	-	Analog
AMS 1956–1957. Ministry of Defense	8 October 1956	1:32,000	50–100	Analog
Interministerial 1973–1986	1973–1986	1:18,000	27–45	Analog
National 1980–1986	1983	1:30,000	45–75	Analog
Olive oil OLISTAT 1997–1998	October 1997, February 1998	1:40,000	100	Analog
SIGPAC 1997–2003	24 September 2002	1:15,000 1:30,000	25–50	Analog
Quinquennial 1998–2003. IGN	2002	1:40,000	100	Analog
PNOA 2006	11 August 2006	1:30,000	45	Analog
PNOA 2009	26 September 2009	1:20,000	22	Digital
PNOA 2012	09 July 2012	1:30,000	45	Digital
PNOA 2015	28 June 2015	1:30,000	45	Digital
PNOA 2018	22 September 2018	1:25,000	34	Digital

The mapping consisted of identifying the contours of the ponds and the landscape geoforms that had been generated on them by the action of geological agents (water, wind, gravity) and by human activity since they were abandoned. Prints of the aerial photographs at a scale of approximately 1:2000 were viewed under a tabletop stereoscope, except for the 1997–1998 flight where the orthophotos were used. All the information was integrated and processed in the ArcGIS Geographic Information System, version 10.7.1 (Esri, Redlands, CA, USA), considering the different format of the data source. Landscape geoforms and mine pond boundaries, identified in the stereo pair images, were digitized and stored in shapefile format and from them sludge mine pond areas were obtained. For geomorphological mapping, the orthophoto of the 2018 flight was used and this interpretation was contrasted with a field survey on 26 July 2021. The perimeter of the ponds was walked to observe the slopes, and east–west parallel transects were also made to observe features from both the north and south ponds. In addition, biological activity data were collected, and a photographic inventory was made.

2.3. Volume, Loss–Gain and Erosion Rate of Sludge and Toxic Element Mobilization

To map and quantify the sludge volume variations between 1954–2009 and 2009–2014, altitude data from the 1954 topographic map (1:25,000 scale and 10 m contour interval) [39] and from the 2009 and 2014 LiDAR flights were used (point density 0.5 points/m^2). The horizontal (RMSE x,y) accuracy of the LiDAR data is $\leq$0.30 m, and the accuracy for the vertical (RMSE z) component is $\leq$0.15 m [30]. The ArcGIS software allowed us to import the x,y,z coordinates of the LiDAR point cloud and convert them into three-dimensional models, from which DTMs were derived. LASTools were used to convert the laz LiDAR data to las format. After that, the LAS dataset vegetation was removed and las format was converted to raster.

In order to calculate the sludge volume in 2009, a reference surface was estimated from the visual analysis of the stereoscopic images of the 1946 and 1956 flights, and it was found that the sludge was deposited on a summit area with flat topography. This area is surrounded by a 1110 m contour line in the georeferenced 1954 topographic map [39]. Therefore, a constant height raster of 1110 m was generated and the 2009 LiDAR data were superimposed onto it. This constant elevation DTM was used as a reference surface to calculate the volume of sludge generated until 2009.

The variation in sludge volume between 1954–2009 and 2009–2014 was estimated from the raster data using the ArcGIS cut and fill tool. Analysis of volume variation between the mine pond border and the surrounding area and between the north and south pond boundary was carried out using polygonal layers of the specific areas. The border between both mine ponds was based on the change in slope of the 2014 LiDAR elevation map. The layers were applied as a mask by using the cut-and-fill tool (Figure 2). The rest of the volumes, for which no mask was generated, were calculated by mathematical relation (e.g., surrounding area contour = 2009 contour − 1983 contour). The uncertainty of the volumes measured was calculated using the arithmetic mean and standard deviation of the data with the ArcGIS statistical tool. This provided the standard error presented here. The error of the volumes estimated by mathematical relations was the sum of the errors of these values.

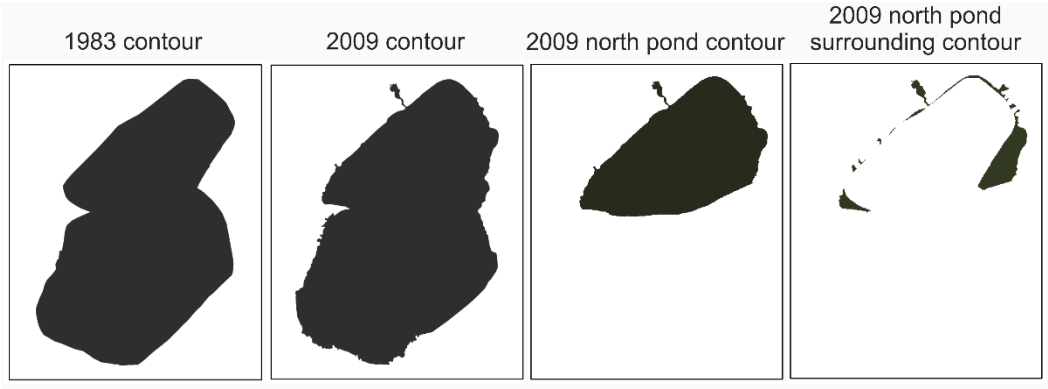

Figure 2. Schematic example of the masks applied with the ArcGIS cut-and-fill tool to calculate the volume difference in specific areas of the pond between 1983 and 2009. The volumes of the south pond and the entire perimeter were calculated by mathematical relations.

Finally, the erosion rate of the ponds and the amount of potentially released toxic elements were calculated through the volumetric balance between 2009 and 2014. To obtain the sludge mass, the dry density was estimated from the metallic content and mineralogical composition of the sludge from Hiendelaencina. In addition, published values of porosity and grain density in sludge from similar mining areas were also used.

3. Results

3.1. Geomorphological Mapping of Mine Tailings

Geomorphologies and deposit characteristics of hydrological, gravitational, wind, biological and anthropic processes were identified in both ponds (Figure 3). Water processes have formed four abrupt gullies in each of the slopes of the north pond which connect to the surface with small river valleys of ephemeral streams. In the south pond, there is an emerging gully on the south–east slope. The eroded sludge transported by water is deposited at the end of the gullies forming alluvial cones (1–2 in Figures 3 and 4). On the slopes of the ponds, the streams flow in rills (4 in Figures 3 and 4). Due to the way in which the ponds were enlarged, two depressions were formed in their central areas where temporary flooding occurs. In the dry season, saline efflorescence precipitates on the sludge (3 in Figures 3 and 4).

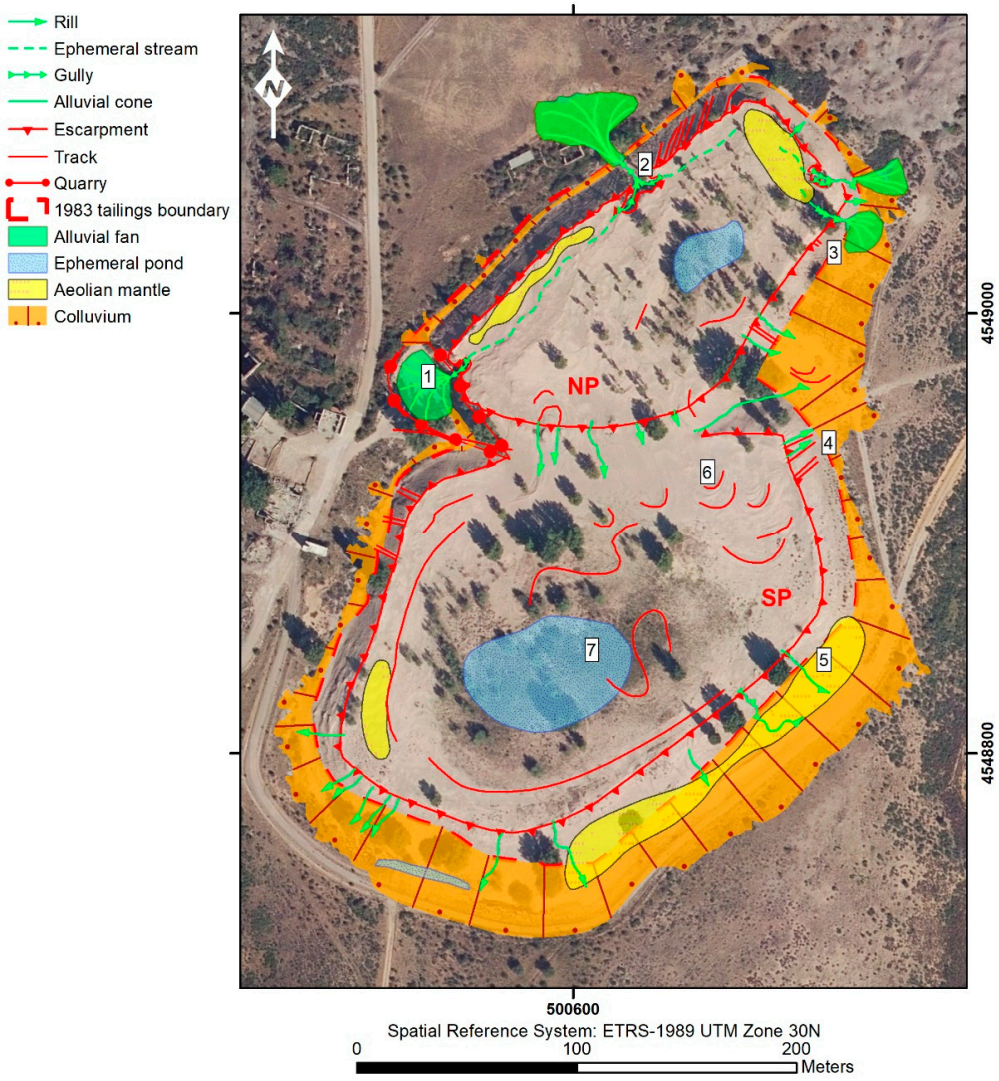

Figure 3. Geomorphological map based on the photointerpretation of the 2018 orthophoto and field observations. Numbers correspond to the shooting position of the photographs shown in Figure 4. 1: Alluvial cone at the mouth of the westernmost gully of the north pond. 2: North pond gully. 3: Saline efflorescence, exposed roots, motorbike tracks and excavated nests on a hillside of the north pond. 4: Rill erosion over motorbike tracks on a hillside of the south pond. 5: Ripples on the eolian mantle that was developed over colluvium of the south pond. 6: Crescent-shaped tracks and mounds due to motorbike racing in the south pond. 7: Vegetation cover in the temporary flooded area of the south pond. NP: North pond or San Carlos 2-mine tailings. SP: South pond or San Carlos 1-mine tailings.

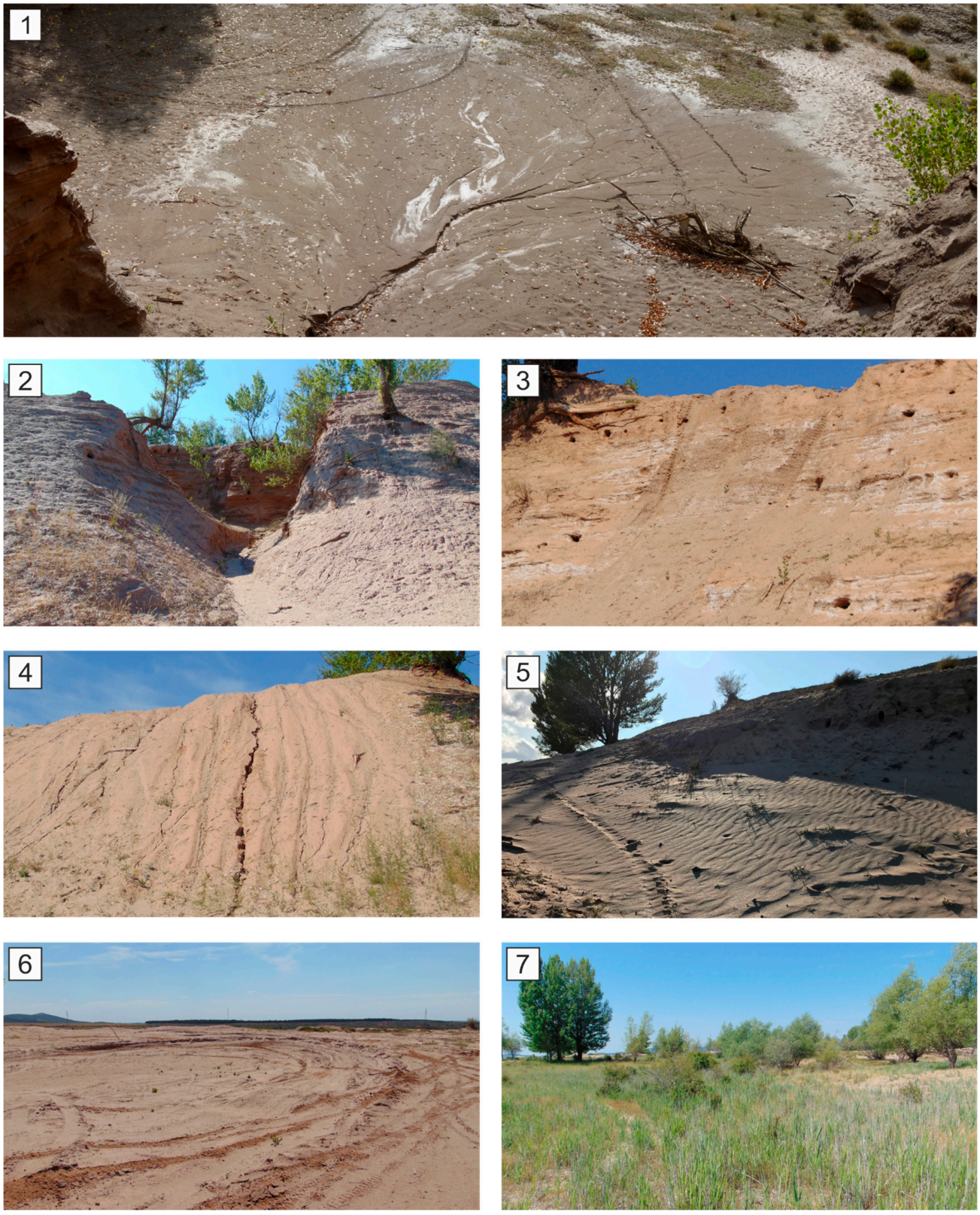

Figure 4. Landforms on the ponds. The numbering of each photograph corresponds to the photograph points in Figure 3. 1: Alluvial cone at the mouth of the westernmost gully of the north pond. 2: North pond gully. 3: Saline efflorescence, exposed roots, motorbike tracks and excavated nests on a hillside of the north pond. 4: Rill erosion over motorbike tracks on a hillside of the south pond. 5: Ripples on the eolian mantle that developed over colluvium of the south pond. 6: Crescent-shaped tracks and mounds due to motorbike racing in the south pond. 7: Vegetation cover in the temporary flooded area of the south pond.

The joint action of hydrological and gravitational processes on the slopes of the ponds has led to their retreat, which is evident by the presence of trees with exposed roots (2–3 in Figures 3 and 4). The south–west-oriented slopes of the south pond are stepped due to the differential erosion of alternating coarser- and finer-grained sludge levels. The eroded sludge is deposited around the perimeter of the ponds, forming a colluvium, the extent of which is greater towards the south (5 in Figures 3 and 4).

The parts of the pond that lack vegetation cover are exposed to the wind during dry periods. This has led to the formation of 2–3 cm thick eolian mantles on which ripples develop (5 in Figures 3 and 4). The grain size of the sludge, based on the USDA textural classification, varies from loamy sand (predominantly medium sand 0.5–0.2 mm or fine sand 0.2–0.05 mm, ~40% by weight) to sandy loam (~48% by weight of silt fraction 0.05–0.002 mm). However, the texture of the eolian mantle deposits is sandy and the majority of the fraction is medium sand (~59% by weight on average). The ripples in the western deposit of the north pond have a N132°E average orientation, while in the eastern deposit of the south pond the ridge direction varies from N112°E to N198°E. These sands are in turn eroded away during the rainy season and transported by ephemeral currents to the alluvial cones, colluvium or depressed areas.

In addition to these geological processes, human activity has modified the ponds, altering the stream processes. Motorbike tracks on the slopes generate preferential paths, which in some cases are across the steepest slope (2–3 in Figures 3 and 4). The surface of both ponds is used as a dirt track, compacting the surface and creating depressions under the tracks, as well as mounds due to the accumulation of material raised by motorcycles and quad bikes from riding (6 in Figures 3 and 4). On the other hand, based on the evolution of the mine tailings over time (Figure 5), it has been possible to identify an area of sludge extraction in the south–west corner of the north pond (Figure 3).

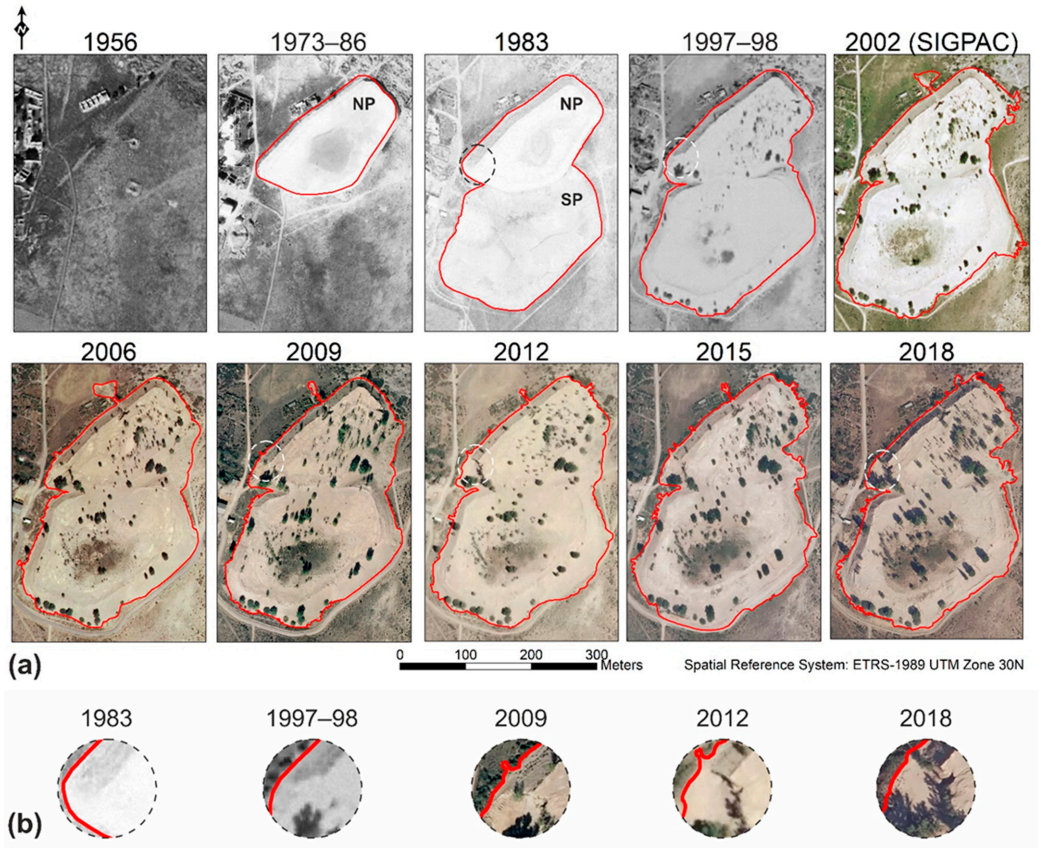

Figure 5. (**a**) Time evolution of the mining ponds of San Carlos. NP, north pond; SP, south pond; red lines, sludge contours. (**b**) Details of the south–west corner of the north pond; dashed circles in (**a**) = where tailings were extracted in a quarry.

Biological activity also moves a small amount of sludge. There are sand martin nests on the slopes of the gullies, bee-eater nests on the more vegetated slopes, and small mammal burrows (3 in Figures 3 and 4). These animals break up and weaken the slopes. On the other hand, in the areas of temporary flooding, as well as in the loose materials of the colluvium, flora species typical of wetlands have developed (7 in Figures 3 and 4). Vegetation cover in the ponds occupies 29.5% of the surface, with herbaceous and shrub plants predominating in the south pond and trees in the north pond.

3.2. Formation and Evolution of Mine Tailings

Photographs from the 1946 and 1956 flights show the remains of the abandoned San Carlos mining complex (Figure 5). Some of these structures were reused during the further processing of the tailings dumps or buried under the sludge ponds. The first presence of sludge is recorded on the 1973–1986 flight. These deposits are associated with the north pond (San Carlos 2), which occupied an area of 22,776 m^2, and in the central part the supernatant accumulated. In the 1983 flight, the increase in height of the north pond and the start of mining work in the south pond (San Carlos 1) can be seen. The total extension is 57,932 m^2 and, by difference, the extension of the south pond (San Carlos 1) is 35,806 m^2 (Table 2). From 1983 to 2018, the area occupied by sludge increased by 31.5% to 76,161 m^2. In all cases, the estimated error is below 1 m (RMSE x,y $\leq$ 1.00 m [30]).

Table 2. Volume (m^3) and area (m^2) of sludge in 2009 (2009 contour), breaking down the values inside (1983 contour) and outside (surrounding area) the 1983 boundary of the ponds.

Mine Pond	2009 Contour		1983 Contour		Surrounding Area	
	Volume	Area	Volume	Area	Volume	Area
North	293,732 ± 108	25,475	279,862 ± 89	22,126	13,869 ± 19	3349
South	338,850 ± 765	42,593	319,078 ± 746	35,806	19,772 ± 1334	6787
North + South	632,582 ± 657	68,068	598,940 ± 657	57,932	33,642 ± 1315	10,136

After the closure of mines at the beginning of the 1990s, changes are recognizable in the new terrain created by the ponds, which are associated with geological, biological and anthropogenic processes, and which progress over time. In the 1997–1998 flight, rills on the southern slope of the south pond, two gullies on the north–east slope of the north pond, isolated trees, and the extraction of sludge in the southwest corner of the north pond are identified (quarry in Figure 3). The area covered by sludge in 1997–1998 increased by 11.5% compared to the perimeter of the mine ponds when they were operational (1983). This is the largest increase detected between two consecutive flights (Table 3). In 2002, the formation of the north–west slope gully stands out, connected with a diffuse stream towards the surface of the deposit and with the alluvial cone on the perimeter. In the south pond, colluvium/eolian mantle deposits are observed towards the south–east, and the more depressed central part begins to be reclaimed by herbaceous-type vegetation. In comparison with the previous flight, the surface occupied by sludge has increased by 5.4%.

Table 3. Area (m^2) of sludge (RMSE x,y $\leq$ 1.00 m [30]).

	1973–1986	1983	1997–1998	2002 SIGPAC	2006	2009	2012	2015	2018
Area	22,776	57,932	64,566	68,054	68,209	68,068	69,538	70,988	68,671

The landforms described above were still in place in 2006, and on the surface of the ponds there are pale patches that could be related to the precipitation of saline efflorescence during summer. However, the most significant changes from previous years are the motorbike tracks along the perimeter of the south pond surface. In the 2009 image, traces of tracks can be seen on the north pond and on the slopes, and a greater number of streams, the formation of the gully on the slope of the quarry, and the greater extension of the

colluvium/eolian mantle in the south–east are also recognized. There is almost no change in the area occupied by sludge in the period 2002–2009. In the 2012 image, the only relevant issue is the change in the hillside in the north pond quarry due to a new sludge extraction. The south–east colluvium/eolian mantle reaches its maximum extent in 2015, and some runoff is identified across it. An average 2.1% increase in sludge area is obtained between 2009–2012 and 2012–2015. Lastly, in 2018 there was a strong erosion in the quarry slope gully, and the rest of the elements already described in the previous subsection can also be recognized. However, sludge surface decreases by 3.3% compared to the previous flight.

Overlapping of the sludge contours of all images shows that the residue movement has not been homogeneous over time (Figure 6). The west, north–west and north–east hillsides have maintained their position as roughly constant, except for the occasional deposition beyond the initial perimeter of the ponds that is associated with stream processes and human activity. However, on the south–east and south hillsides, there has been a greater displacement of sludge due to the formation of colluvium/eolian mantle. Some areas show a higher settlement of sludge removed in past, e.g., the alluvial cone at the north–west hillside of the north pond. This is due to the growth of vegetation on the sludge after deposition. While the area occupied by the sludge was changing, the position of scarp hillsides receded by an average retreat of 3 m from 1983 to 2018, reaching up to 10 m in the gully areas.

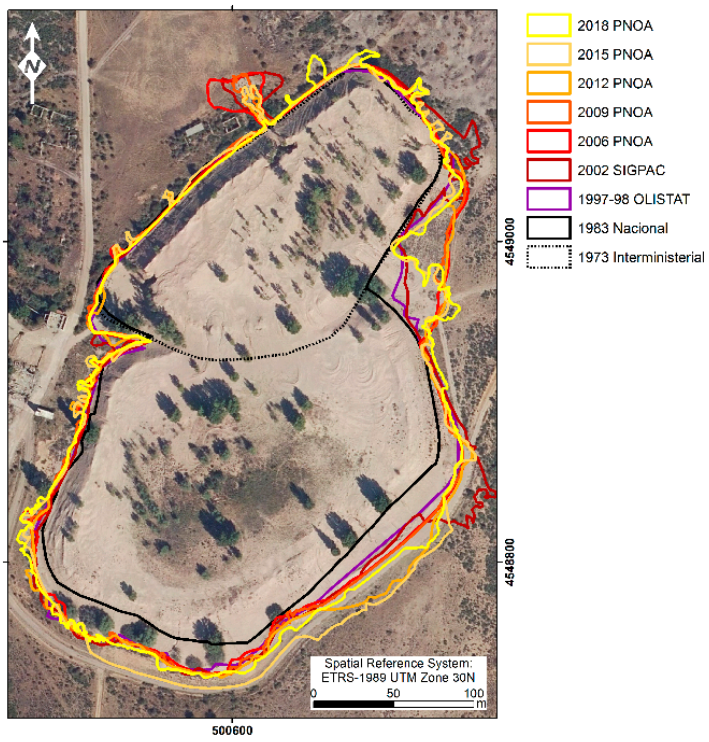

Figure 6. Sludge contours over time on the orthophoto from the 2018 flight.

The mixed action of natural (surface erosion) and anthropic processes not only modifies the extent occupied by the sludge, but also determines the value of the pond slopes (Figure 7). The hillsides of the north pond had slopes greater than 60% in 2009 that had increased by 2014. In contrast, the hillsides of the south pond had slopes in the range of 30–60%, locally steepening to more than 60%, which tended to decrease. These differences, together with the greater height of the north pond compared to the south pond, may be the reason why the north pond has steep gullies on its slopes, which are connected to small valleys on the surface, while the south pond has only rills. In that period, the valleys were excavated by the ephemeral streams, the inland depressions with temporary flooding

deepened and even slightly increased in size, and the tracks caused by motorbikes also became more pronounced.

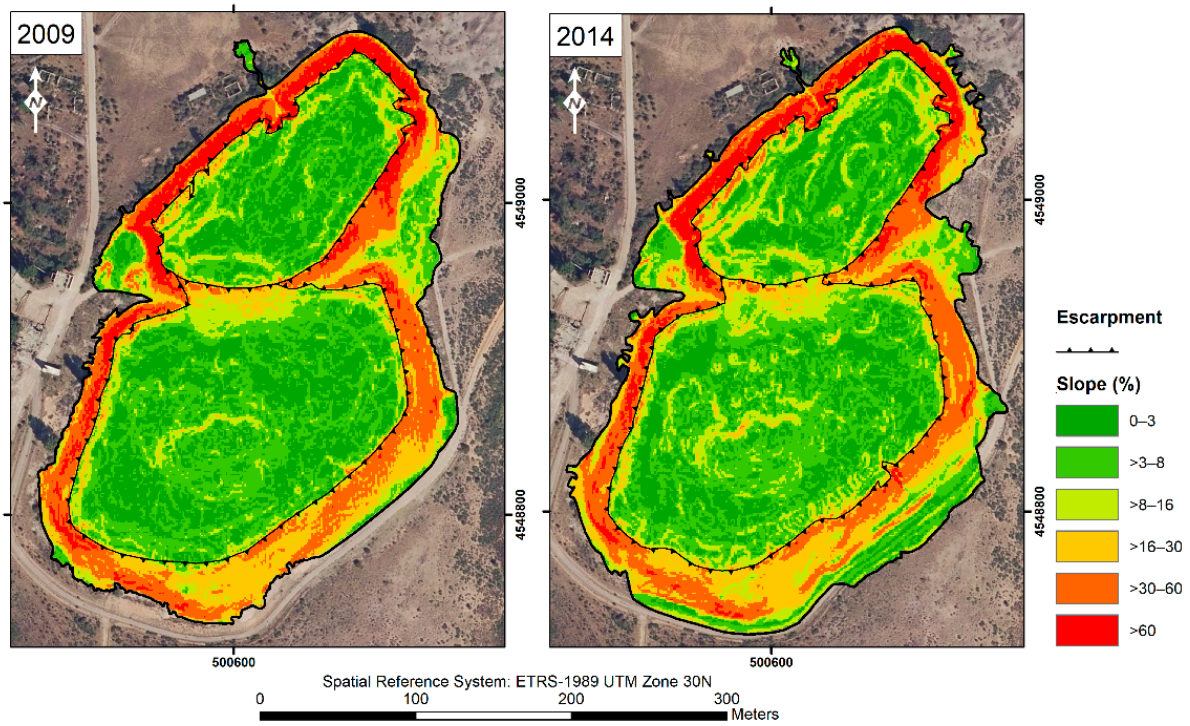

Figure 7. Slope map for both ponds corresponding to the light detection and ranging (LiDAR) flights of 2009 and 2014.

3.3. Volume, Loss–Gain and Erosion Rate of Sludge

To quantify the amount of sludge movement since mining activity ceased, and since there is no detailed altitudinal information prior to 2009, it has been assumed that the eroded material was deposited in the surrounding area closest to the ponds. In 2009, there was 632,582 ± 754 m^3 of sludge distributed over an area of 68,068 m^2. This volume and those of each pond (Table 2) are equivalent to the ones listed in the IGME catalogue file [29]. Considering the initial boundary of the ponds in 1983 (57,932 m^2), the amounts of sludge inside the 1983 contour and in the surrounding area in 2009 were 598,941 m^3 and 33,642 m^3, respectively. Therefore, between 1983 and 2009, 5.3% of the total volume of sludge was eroded from the ponds and deposited into the surrounding 10,136 m^2, increasing the occupied area by 17.5% (Figure 6). The volume of sludge movement from the south pond to its surrounding zone (5.8%) is higher than that from the north pond (4.7%). Similarly, the increase in the area occupied by sludge around the south pond (19.0%) also exceeds that of the north pond (15.1%).

Based on the altitude data collected by LiDAR flights, the distribution of sludge loss and gain between 2009 and 2014 has been quantified and mapped (Table 4 and Figure 8). Within the original perimeter of the ponds (1983 contour), the volumes of lost and gained sludge are similar, but the areas affected are larger in the south pond. The surrounding zone of the south pond has the highest values for calculated volumes and areas with loss and gain, but this area increased in size from 2009 to 2014. The combined action of the erosive agents over six years has produced a net loss of 8849 m^3 of sludge, with a retention of 282 m^3 in the surrounding area of the ponds.

Table 4. Sludge loss and gain between 2009 and 2014 expressed in volume (m^3) and area (m^2), with the breakdown of values inside (1983 contour) and outside (surrounding area) the 1983 boundary of the ponds.

	Mine Pond	2009–2014 Contour		1983 Contour		Surrounding Area	
		Volume	Area	Volume	Area	Volume	Area
Loss	North	−5902 ± 75	20,087	−5812 ± 78	19,005	−89 ± 3	1082
	South	−6923 ± 33	30,929	−5424 ± 39	25,715	−1498 ± 61	5214
	North + South	−12,825 ± 112	51,016	−11,237 ± 105	44,720	−1588 ± 22	6296
Gain	North	1519 ± 26	6470	1076 ± 32	4001	442 ± 17	2469
	South	2457 ± 190	14,923	1029 ± 190	8997	1427 ± 191	5926
	North + South	3976 ± 189	21,393	2106 ± 189	12,998	1870 ± 191	8395
Balance	North + South	−8849 ± 135	-	−9130 ± 117	-	281 ± 74	-

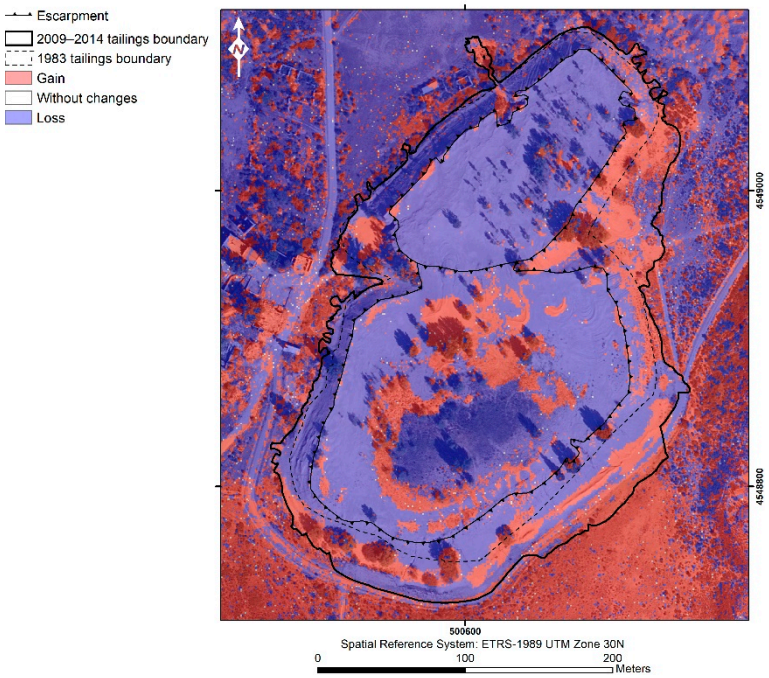

Figure 8. Sludge loss and gain distribution map between 2009 and 2014.

3.4. Toxic Elements Mobilized into the Environment

Once the net loss of sludge is known, it is possible to estimate the tonnes of potentially hazardous metals that have been eroded and transported to the surrounding areas of the ponds during this 6-year period. With this aim in mind, we used the metal contents and mineralogical composition of the ponds obtained by X-ray diffraction and published by [40]. In this work [40], tailings were collected with an Eijkelkamp soil core manual sampler for undisturbed samples, with a known volume and diameter. Twenty samples were collected with a vertical constant spacing of 50 cm from the pond surface to a depth of 9.5 m along the gully vertical hillsides at the SW corner of the north mine pond. This procedure, also used in the La Naya mine pond [23], allows us to determine variations in element contents from the surface to the bottom and, therefore, work with representative and average values.

From the mineralogical composition of the sludge [40], the density of the solid phase was calculated (Table 5). Porosity and grain density data from sludge from similar ponds in Sweden [41], Ireland [42] and South Africa [43] reveal the existence of a linear correlation between both parameters (Figure 9). Non-linear models were also tested but they did not provide significantly better results. From the linear equation and our calculated grain density values, we obtained the porosity values that were needed for the subsequent calculation of dry density values (Table 5).

Table 5. Main physical features of the mine tailings and amounts of metals eroded.

Pond	Grain Density (t/m^3)	Dry Density (t/m^3)	Mass (t)	Element Amount (t)								
				Ag	As	Cr	Cu	Ni	Pb	Sb	Zn	Σ
North	2.87	1.706 ± 0.053	7477 ± 404	0.1 ± 0.01	0.9 ± 0.05	0.4 ± 0.02	0.1 ± 0.01	0.1 ± 0.01	1.3 ± 0.07	0.2 ± 0.01	1.2 ± 0.06	4.2 ± 0.2
South	2.92	1.705 ± 0.039	7615 ± 553	0.1 ± 0.01	1.8 ± 0.11	0.3 ± 0.02	0.2 ± 0.01	0.1 ± 0.01	1.7 ± 0.1	0.3 ± 0.02	1.7 ± 0.1	6.1 ± 0.4

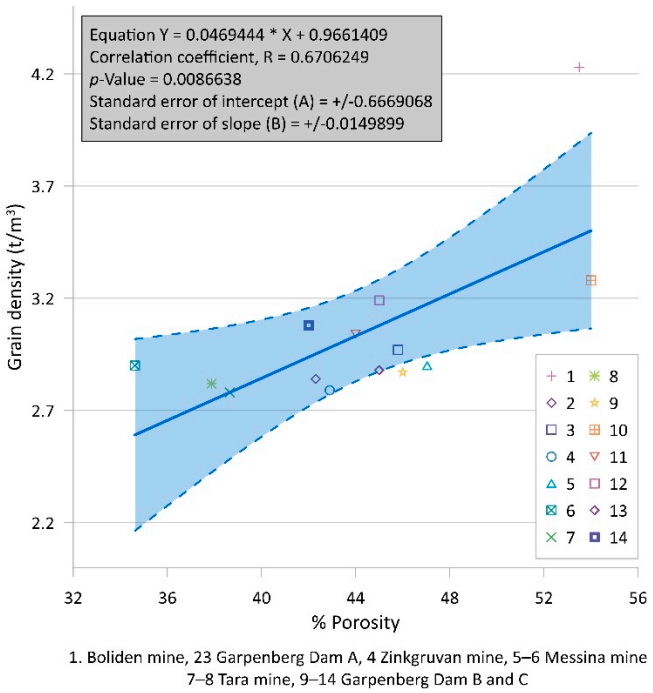

Figure 9. Grain density vs. porosity plot and parameters of the linear fit. The fit has been computed with a 95% confidence (blue zone). Data from Mansson [41], Quille and O'Kelly [42] and Mhlongo [43].

Finally, with this dry density value and the volume of net sludge loss (Table 4), the total mass eroded from the ponds was calculated, followed by the tonnes of potentially hazardous metals eroded. A value of 4.2 ± 0.2 t of metals was calculated for the north pond, and for the south pond 6.1 ± 0.4 t of metals were eroded and deposited in the surrounding areas. Particularly noteworthy are the values of As (2.7 ± 0.16 t), Pb (3 ± 0.17 t) and Zn (2.9 ± 0.16 t).

Considering the estimated density for these sludge deposits of 1,705 ± 0.046 t/m^3 and a pond surface of 7.27 ha, the erosion rate during this period was 346 ± 9 t/ha*year. The loss of sludge on the surface of the ponds is related to the erosive action of the surface streams and the wind, increased by the breakdown of material by motorbike riders. On the surface of the south pond there are areas of sludge gain build-up (Figure 8). Those areas that are close to the north pond coincide with mounds created by motorbikes, while in the areas bordering the central zone of temporary flooding, particles are retained by the higher sludge moisture content and vegetation cover. Sludge loss on the slopes is caused by surface runoff processes (in sheets, rills, gullies) and gravitational processes. Sludge gain in the surrounding zone is associated with sedimentation in the alluvial cones and colluvium.

4. Discussion

The combination of UAVs and terrestrial photogrammetric methods over recent years is revealing as an accurate procedure to obtain 3D MDTs that are the closest approximations of surface morphology [14,15,17,20]. With this approach, more than one z-coordinate per xy set can be obtained and, thus, complex topographies, such as the ones in gullies with undercut walls, are detected and modelled with detail. On the other hand, the spatial and

temporal coverage of satellite data is increasingly available in some countries, and 2.5D models can be obtained over large territories [18,44]. In this study, we have estimated the erosion dynamics of the Hiendelaencina abandoned mine tailings from a methodological approach, combining the use of aerial photographs, orthophotos and satellite data [30]. Although there are a scarcity of LiDAR data to estimate sludge erosion rate accurately, the two DTMs obtained from satellite imagery are helpful for a preliminary estimation. Furthermore, erosion rates are usually higher in mining deposits than in natural landscapes [12,21]. Thus, large variations in elevation can be detected in the terrain over a period of a few years. Field work was essential to recognize rills from motorcycle tracks on some slopes or mapping eolian mantles, and check that there were no significant differences in landscape forms from those already observed in the photointerpretation. Therefore, surface processes affecting a mine site can be better understood with the integration of different remote sensing imagery and data. However, erosion dynamics cause the dispersion of pollutants in metallic mineral districts, and tailings characteristics can also be used to identify environmental pollution problems [1–9]. We obtained the amount of metals dispersed to the surrounding areas of the mine ponds by using their physicochemical features.

Several studies demonstrate the environmental impact of the erosion of mining deposits and the displacement of tailings outside different mining areas through surface runoff [4,5,10]. The amount of material transported depends on variables such as grain size and amount of precipitation [45]. In the Cartagena–La Unión mining district (SE Spain), 2.14 kg/m^2 of mining sludge were lost after a 60.5 mm rainfall event [8]. However, in the Santa Engracia mine (Guadalajara, Spain), water erosion processes have been identified with lower precipitation values (8.2 mm in a rain event on 25 August 2007) [46]. The highest rainfall episodes in Hiendelaencina are not very severe (46 mm/day on average) [38], but they have generated very pronounced erosive geoforms (gullies, valleys, rills) in the mining ponds since they were abandoned, as well as hillside scarp retreating and the formation of colluviums (Figures 3–5). High amounts of toxic and mobile elements, such as arsenic, have been found in the sediments of the Cal and Diógenes streams, confirming the effective transport of tailings by surface runoff from mines and slagheaps [47].

Although no erosional landforms associated with gravitational processes on the hillsides have been identified in the Hiendelaencina ponds, the colluvium may also include material accumulated by gravity. These processes should be more noticeable on the steep slopes of the gullies and hillsides of the north pond (Figure 4). Catastrophic gravitational processes are responsible for the breakage of pond dams with steep slopes and large volumes of sludge, as seen in the case of the Aznalcóllar mining pond [48]. However, the smaller size of the two Hiendelaencina deposits and their good mechanical stability reduce the probability of occurrence of this type of phenomenon.

Much of the finer mining waste in semi-arid areas is transported over long distances by high winds [3,4,7]. The collisions that occur between particles due to wind saltation modify the cohesion of the sludge, allowing the separation of the finer fractions that include heavy metals and are displaced by winds of 14.4–25.2 km/h [49]. The effective wind that can move sludge from the San Carlos ponds to the urban center of Hiendelaencina occurs from mid-June to September, with a north–west to south–east orientation and average speeds of 12.9 km/h, which can reach 25 km/h in June [38]. The ridges of eolian mantle ripples are parallel to the slope of the hillside from which they are formed (Figure 4). This arrangement is consistent with small shifts in the prevailing wind directions around the ponds. On the other hand, the dominantly sandy grain size of the sludge with the small presence of finer fractions suggests that the wind has blown the latter away. If this released fraction contains metallic particles, this could pose a health risk to the inhabitants in the surrounding area.

Although some plants can extract metals from the soil and bioaccumulate them, native species colonizing the studied mining ponds are not effective in fixing these elements [50]. Vegetation improves water retention and soil structure, and helps reduce erosion processes [51], but in semi-arid climates a minimum cover of 50% is needed, especially of the

herbaceous type [52]. The lower vegetation cover in the Hiendelaencina ponds (29.5%) would, therefore, be insufficient to prevent sludge erosion. However, the distribution of vegetation is not consistent and its contribution could be varied. There is a predominance of zones with isolated growing trees and shrubs, but on steep slopes (>30°) their roots usually become exposed by erosion. On the other hand, there is a higher density of vegetation, including herbaceous species, in the central depressed area of the south pond, which is subject to temporary flooding and, therefore, better retains the mobilized tailings. Steep hillsides in abandoned mines register maximum erosion rates due to the higher surface runoff along rills and gullies [21,53]. Recent studies suggest geomorphic mining reclamation to mitigate the loss of mine waste [19]. The slope of linear hillsides should be lessened to 32% or transformed to a concave profile, and the surface should be covered with topsoil. This integrated management of topography and soil allows spontaneous vegetation colonization and the stabilization of hillsides.

The grain density, porosity and dry density values obtained for the sludge from the Hiendelaencina mining ponds are similar to those published by other authors for this type of mining sludge [23,54]. Although the content of potentially hazardous metals in these ponds is not significantly high when compared to similar deposits in other mining districts in Spain [6,23,55,56], significantly high net amounts of mining sludge lost through erosion have been found (more than 10 t of metals). This is due to the high rate of erosion calculated from these deposits (346 $\pm$ 9 t/ha*year). The estimated erosion rate in abandoned deposits in semi-arid areas ranges between 100 and 150 t/ha*year (NW Mexico [57], SE Spain [10]). The higher value calculated in Hiendelaencina may be linked to the coarser granulometry of the sludge and to the specific climatic, geomorphological, and anthropic characteristics of the region. Higher annual rainfall can lead to a larger amount of sludge movement. As the ponds are in a flat, elevated and completely open uphill area, the entire sludge perimeter is exposed to the combined effects of water, wind and gravity. In addition, the recreational use of these deposits for motorbike racing strongly alters the cohesion of the sludge, increasing erosion. Therefore, considering climate change, where periods of drought and torrential rains are likely to become increasingly intense, measures to restore and/or stabilize the ponds should be undertaken to reduce the high rate of erosion and the dispersion of potentially toxic metals.

5. Conclusions

The study of geomorphological processes in abandoned mining sludge ponds and their time evolution, together with the estimation of erosion rates from aerial imagery and LiDAR data, has revealed the state of degradation of these deposits, as well as the movement of potentially toxic materials into the environment, and provides information for planning future restoration. In the tailings of the Hiendelaencina mining district there are hydrological, wind, gravitational and anthropic processes that erode the sludge and deposit it at the foot of the hillsides. Although vegetation cover has been developing on the surface of the ponds, its low density and irregular distribution are not enough to prevent particle movement. The climatic, geomorphological and anthropic characteristics of the region determine the high rate of erosion recorded, and measures should be undertaken to prevent potential damage to population living nearby.

Author Contributions: S.M.-V., I.R.-S., D.G.-O., T.M.-C. and C.d.I.-S.J. performed the conceptualization. S.M.-V., I.R.-S. and N.R.-S. conducted the investigation, wrote the original draft, and prepared the data visualization. D.G.-O., T.M.-C. and C.d.I.-S.J. participated in the result analysis, revised the manuscript, and provided valuable comments and suggestions. S.M.-V. is responsible for project administration and funding acquisition. All authors have read and agreed to the published version of the manuscript.

Funding: This research was funded by Comunidad de Madrid and Universidad Rey Juan Carlos, grant number M2167.

Data Availability Statement: Not applicable.

Acknowledgments: The authors thank the "Hiendelaencina Silver Mining Interpretation Center" for the logistical support provided during the development of this work. The authors wish to thank also two anonymous reviewers for their useful suggestions, which have helped to improve the manuscript.

Conflicts of Interest: The authors declare no conflict of interest.

References

1. Robles-Arenas, V.M.; Rodríguez, R.; García, C.; Manteca, J.I.; Candela, L. Sulphide–mining impacts in the physical environment: Sierra de Cartagena–La Unión (SE Spain) case study. *Environ. Geol.* **2006**, *51*, 47–64. [CrossRef]
2. Rodríguez, R.; Gómez de las Heras, J. Los residuos de la industria extractiva en España. Distribución geográfica y problemática ambiental asociada. In *Los Residuos Minero-Metalúrgicos en el Medio Ambiente*; Rodríguez, R., García-Cortés, A., Eds.; Instituto Geológico y Minero de España: Madrid, Spain, 2006; Volume 11, pp. 3–25. ISBN 84-7840-655-5.
3. Meza-Figueroa, D.; Maier, R.M.; De la O-Villanueva, M.; Gómez-Alvarez, A.; Moreno-Zazaueta, A.; Rivera, J.; Campillo, A.; Grandlic, C.J.; Anaya, R.; Palafox-Reyes, J. The impact of unconfined mine tailings in residential areas from a mining town in a semi-arid enviromen: Nacozari, Sonora, Mexico. *Chemosphere* **2009**, *77*, 140–147. [CrossRef] [PubMed]
4. Boussen, S.; Sebei, A.; Soubrand-Colin, M.; Bril, H.; Chaabani, F.; Abdeljaouad, S. Mobilization of lead–zinc rich particles from mine tailings in northern Tunisia by aeolian and run–off processes. *Bull. Soc. Geol. Fr.* **2010**, *181*, 459–471. [CrossRef]
5. Sims, D.B.; Hooda, P.S.; Gillmore, G.K. Mining activities and associated environmental impacts in arid climates: A literature review. *Environ. Pollut.* **2013**, *2*, 22–43. [CrossRef]
6. Martín-Crespo, T.; Gómez-Ortiz, D.; Martín-Velázquez, S.; Esbrí, J.M.; De Ignacio-San José, C.; Sánchez-García, M.J.; Montoya-Montes, I.; Martín-González, F. Abandoned mine tailings in cultural itineraries: Don Quixote Route (Spain). *Eng. Geol.* **2015**, *197*, 82–93. [CrossRef]
7. Doumas, P.; Munoz, M.; Banni, M.; Becerra, S.; Bruneel, O.; Casiot, C.; Cleyet-Marel, J.-C.; Gardon, J.; Noack, Y.; Sappin-Didier, V. Polymetallic pollution from abandoned mines in Mediterranean regions: A multidisciplinary approach to environmental risks. *Reg. Environ. Change* **2018**, *18*, 677–692. [CrossRef]
8. Martínez-López, S.; Martínez-Sánchez, M.J.; Pérez-Sirvent, C. Do old mining areas represent an environmental problem and health risk? A critical discussion through a particular case. *Minerals* **2021**, *11*, 594. [CrossRef]
9. García, C.; Riberón-Zaldívar, A.B.; Carménate, J.A.; Rodríguez, R. Buenas prácticas y aplicación de medidas correctoras en áreas afectadas por actividades minero–metalúrgicas. In *Los Residuos Minero-Metalúrgicos en el Medio Ambiente*; Rodríguez, R., García-Cortés, A., Eds.; Instituto Geológico y Minero de España: Madrid, Spain, 2006; Volume 11, pp. 555–587. ISBN 84-7840-655-5.
10. Martín Duque, J.F.; Zapico, I.; Oyarzun, R.; López García, J.A.; Cubas, P. A descriptive and quantitative approach regarding erosión and development of landforms on abandoned mine tailings: New insights and enviromental implications from SE Spain. *Geomorphology* **2015**, *239*, 1–16. [CrossRef]
11. Sánchez-Donoso, R.; Martín-Duque, J.F.; Crespo, E.; Higueras, P.L. Tailing's geomorphology of the San Quintín mining site (Spain). *Environ. Earth Sci.* **2019**, *78*, 166. [CrossRef]
12. Tarolli, P.; Sofia, G. Human topographic signatures and derived geomorphic processes across landscapes. *Geomorphology* **2016**, *255*, 140–161. [CrossRef]
13. Poesen, J.; Nachtergaele, J.; Verstraeten, G.; Valentin, C. Gully erosion and environmental change: Importance and research needs. *Catena* **2003**, *50*, 91–133. [CrossRef]
14. Peter, K.D.; d'Oleire-Oltmanns, S.; Ries, J.B.; Marzolff, I.; Ait Hssaine, A. Soil erosion in gully catchments affected by land-levelling measures in the Souss Basin, Morocco, analysed by rainfall simulation and UAV remote sensing data. *Catena* **2014**, *113*, 24–40. [CrossRef]
15. Stöcker, C.; Eltner, A.; Karrasch, P. Measuring gullies by synergetic application of UAV and close range photogrammetry—A case study from Andalusia, Spain. *Catena* **2015**, *132*, 1–11. [CrossRef]
16. Moudry, V.; Gdulova, K.; Fogl, M.; Klapště, P.; Urban, R.; Komarek, J.; Moudra, L.; Štroner, M.; Bartak, V.; Solsky, M. Comparison of leaf-off and leaf-on combined UAV imagery and airborne LiDAR for assessment of a post-mining site terrain and vegetation structure: Prospects for monitoring hazards and restoration success. *Appl. Geogr.* **2019**, *104*, 32–41. [CrossRef]
17. Frankl, A.; Stal, C.; Abraha, A.; Nyssen, J.; Rieke-Zapp, D.; DeWulf, A.; Poesen, J. Detailed recording of gully morphology in 3D through image-based modelling. *Catena* **2015**, *127*, 92–101. [CrossRef]
18. Emel, J.; Plisinski, J.; Rogan, J. Monitoring geomorphic and hydrologic change at mine sites using satellite imagery: The Geita Gold Mine in Tanzania. *Appl. Geogr.* **2014**, *54*, 243–249. [CrossRef]
19. Martín-Moreno, C.; Martín Duque, J.F.; Nicolau Ibarra, J.M.; Hernando Rodríguez, N.; Sanz Santos, M.A.; Sánchez Castillo, L. Effects of topography and surface soil cover on erosion for mining reclamation: The experimental spoil heap at El Machorro mine (Central Spain). *Land Degrad. Develop.* **2016**, *27*, 145–159. [CrossRef]
20. Park, S.; Choi, Y. Applications of Unmanned Aerial Vehicles in Mining from Exploration to Reclamation: A Review. *Minerals* **2020**, *10*, 663. [CrossRef]
21. Trabucchi, M.; Puente, C.; Comin, F.A.; Olague, G.; Smith, S.V. Mapping erosion risk at the basin scale in a Mediterranean environment with opencast coal mines to target restoration actions. *Reg. Environ. Change* **2012**, *12*, 675–687. [CrossRef]

22. Hambali, R.; Wahyuni, S. The potential for land erosion due to primary tin mining in Bangka Island. *IOP Conf. Ser. Earth Environ. Sci.* **2021**, *926*, 012072. [CrossRef]
23. Martín-Crespo, T.; Martín-Velázquez, S.; Gómez-Ortiz, D.; De Ignacio-San José, C.; Lillo-Ramos, J. A geochemical and geophysical characterization of sulfide mine ponds at the Iberian Pyrite Belt (Spain). *Water Air Soil Poll.* **2011**, *217*, 387–405. [CrossRef]
24. Montoya-Montes, I.; Cano-Bermejo, L.; Sánchez-García, M.J.; de Ignacio-San José, C.; Martín-Velázquez, S.; Gómez-Ortiz, D.; Martín-Crespo, T.; Martín-González, F. Formación de cuerpos dunares a partir de lodos mineros mina de San Quintín (Ciudad Real, España). *Geotemas* **2012**, *13*, 1487–1490.
25. López Gómez, A. El distrito minero de Hiendelaencina (Guadalajara). *Cuad. Geogr.* **1969**, *6*, 211–250.
26. Calvo, M.; Sevillano, E. Hiendelaencina, Spain. *Miner. Rec.* **1992**, *23*, 241–249.
27. Martínez Frías, J. The Hiendelaencina mining district (Guadalajara, Spain). *Miner. Depos.* **1992**, *27*, 206–212. [CrossRef]
28. Arlandi Rodríguez, M.; Calvo Rebollar, M.; López Ramos, F.; Maturana Campos, S.; Sainz de Baranda Graf, B. Hiendelaencina, el filón rico. *Bocamina Rev. Miner. Yacim. Esp.* **1995**, *1*, 4–28.
29. Instituto Geológico y Minero de España (IGME). Inventario Nacional de Depósitos de Lodos. 2002. Available online: https://info.igme.es/balsas/ (accessed on 25 May 2021).
30. Instituto Geográfico Nacional (IGN). Centro Nacional de Información Geográfica. 2021. Available online: https://www.cnig.es (accessed on 24 May 2021).
31. Junta de Comunidades de Castilla la Mancha (JCCM). Centro Cartográfico de Castilla-La Mancha. 2021. Available online: https://castillalamancha.maps.arcgis.com/ (accessed on 24 May 2021).
32. Concha, A.; Oyarzun, R.; Lunar, R.; Sierra, J.; Doblas, M.; Lillo, J. The Hiendelaencina epithermal silver–base metal district, Central Spain: Tectonic and mineralizing processes. *Miner. Depos.* **1992**, *27*, 83–89. [CrossRef]
33. De Pablo, M.A.; de Pablo, J.C.; Paniego, M.J. Proyecto de recuperación del entorno de la mina de plata San Carlos (Hiendelaencina, Guadalajara). *Metall* **2013**, *20*, 53–64.
34. Chías, P.; Abad, T. Hiendelaencina: Imagen y construcción del territorio y del paisaje a través de la cartografía histórica. In *Minas de Plata de Hiendelaencina. Territorio, Patrimonio y Paisaje*; Rosas, Á.L., Ed.; Universidad de Alcalá de Henares: Alcalá de Henares, Spain, 2014; pp. 55–75.
35. Gobierno de Castilla la Mancha. ZEC–ZEPA Sierra de Ayllón ES0000104–ES0000488. Red Natura 2000. 2020. Available online: https://www.castillalamancha.es/gobierno/agrimedambydesrur/estructura/dgapfyen/rednatura2000/liczepaES0000164-ES0000488 (accessed on 24 May 2021).
36. Chazarra, A.; Flórez, E.; Peraza, B.; Tohá, T.; Lorenzo, B.; Criado, E.; Moreno, J.V.; Romero, R.; Botey, R. *Mapas Climáticos de España (1981–2010) y Eto (1996–2016)*; Ministerio para la Transición Ecológica—Agencia Estatal de Meteorología: Madrid, Spain, 2018.
37. Agencia Española de Meteorología (AEMET). Open Access Meteorological Data. 2010. Available online: http://www.aemet.es/es/datos_abiertos/AEMET_OpenData (accessed on 1 June 2021).
38. Weather Spark. El Clima Promedio en Hiendelaencina, España. 2021. Available online: https://es.weatherspark.com/y/37079/Clima-promedio-en-Hiendelaencina-Espa%C3%B1a-durante-todo-el-a%C3%B1o (accessed on 14 June 2021).
39. Instituto Geográfico Nacional (IGN). *Mapa Topográfico del Municipio de Hiendelaencina 1:25,000*; Instituto Geográfico Nacional: Madrid, Spain, 1954.
40. Pryimak, V. Caracterización Geoquímica de la Balsa de Lodos de la Mina de Hiendelaencina (Guadalajara). Bachelor's Thesis, Universidad Rey Juan Carlos, Madrid, Spain, 2021.
41. Mansson, E. Investigation of Particle Sizes, Beach Profiles and Compounds in Tailings Dams. Master's Thesis, Lund University, Lund, Sweden, 2014.
42. Quille, M.E.; O'Kelly, B.C. Geotechnical properties of zinc/lead mine tailings from Tara Mines, Ireland. In Proceedings of the ASCE GeoShanghai, Shanghai, China, 3–5 June 2010; Volume 204, pp. 111–117.
43. Mhlongo, S.E.; Makatu, F.L.; Malaza, N.K.; Ramalata, A.T. Evaluation of copper tailings from the abandoned Messina Mine for possible reuse in recreational projects, South Africa. *J. Degrad. Min. Lands Manag.* **2022**, *9*, 3359–3366. [CrossRef]
44. Rodríguez-Santalla, I.; Gomez-Ortiz, D.; Martín-Crespo, T.; Sánchez, M.J.; Montoya-Montes, I.; Martín-Velázquez, S.; Barrio, F.; Serra, J.; Ramírez-Cuesta, J.M.; Gracia, F.J. Study and Evolution of the Dune Field of La Banya Spit in Ebro Delta (Spain) Using LiDAR Data and GPR. *Remote Sens.* **2021**, *13*, 802. [CrossRef]
45. Benito, G.; Benito-Calvo, A.; Gallart, F.; Martín-Vide, J.P.; Regües, D.; Bladé, E. Hydrological and geomorphological criteria to evaluate the dispersion risk of waste sludge generated by the Aznalcollar mine spill (SW Spain). *Environ. Geol.* **2001**, *40*, 417–428. [CrossRef]
46. Sanz, M.A.; Martín-Duque, J.F.; Martín-Moreno, C.; Lucía, A.; Nicolau, J.M.; Pedraza, J.; Sánchez, L.; Ruiz, R.; García, A. Silica sand slope gullying and mining in Central Spain: Erosion processes and geomorphic reclamation of contour mining. In *Geo–Environment and Landscape Evolution III*; Mander, U., Brebbia, C.A., Martin-Duque, J.F., Eds.; WIT PRESS: Boston, MA, USA, 2008; pp. 4–14. ISBN 978-1-84564-117-7.
47. De Vos, W.; Viaene, W. Geochemical study of soils and metallogenetic implications at Hiendelaencina, Guadalajara, Spain. *Miner. Depos.* **1980**, *15*, 87–89. [CrossRef]
48. Alonso, E.E.; Gens, A. Aznalcóllar dam failure. Part 2: Stability conditions and failure mechanism. *Géotechnique* **2006**, *56*, 185–201. [CrossRef]

49. Ojelede, M.E.; Annegarn, H.J.; Kneen, M.A. Evaluation of aeolian emissions from gold mine tailings on the Witwatersrand. *Aeolian Res.* **2011**, *3*, 477–486. [CrossRef]
50. Wong, M.H. Ecological restoration of mine degraded soils, with emphasis on metal contaminated soils. *Chemosphere* **2003**, *50*, 775–780. [CrossRef]
51. Conesa, H.M.; Faz, A.; Arnaldos, R. Heavy metal accumulation and tolerance in plants from mine tailings of the semiarid Cartagena–La Unión mining district (SE Spain). *Sci. Total Environ.* **2006**, *366*, 1–11. [CrossRef]
52. Moreno-de las Heras, M.; Merino-Martín, L.; Nicolau, J.M. Effect of vegetation cover on the hydrology of reclimed mining soils under Mediterranean-Continental climate. *Catena* **2009**, *77*, 39–47. [CrossRef]
53. Howard, E.J.; Loch, R.J. Acceptable erosion rates for mine waste landform rehabilitation modelling in the Pilbara, Western Australia. In *Mine Closure*; Fourie, A.B., Tibbett, M., Eds.; Australian Centre for Geomechanics: Perth, WA, Australia, 2019; pp. 1545–1559. ISBN 978-0-9876389-3-9.
54. Bhanbhro, R. Mechanical Properties of Tailings: Basic Description of a Tailings Material from Sweden. Licentiate Thesis, Luleå University of Technology, Luleå, Sweden, 2014. Available online: https://www.researchgate.net/publication/265296679_Mechanical_Properties_of_Tailings_Basic_Description_of_a_Tailings_Material_from_Sweden (accessed on 1 June 2021).
55. Martín-Crespo, T.; Gómez Ortiz, D.; Martín Velázquez, S.; Martínez Pagán, P.; De Ignacio, C.; Lillo, J.; Faz, A. Geoenvironmental characterization of unstable abandoned mine tailings combining geophysical and geochemical methods (Cartagena–La Union district, Spain). *Eng. Geol.* **2018**, *232*, 135–146. [CrossRef]
56. Martín-Crespo, T.; Gómez-Ortiz, D.; Martín-Velázquez, S.; Martínez-Pagán, P.; de Ignacio-San José, C.; Lillo, J.; Faz, A. Abandoned mine tailings afecting riverbed sediments in the Cartagena—La Union district, mediterranean coastal area (Spain). *Remote Sens.* **2020**, *12*, 2042. [CrossRef]
57. Peña-Ortega, M.; Del Rio-Salas, R.; Valencia-Sauceda, J.; Mendívil-Quijada, H.; Minjarez-Osorio, C.; Molina-Freaner, F.; De la O-Villanueva, M.; Moreno-Rodríguez, V. Enviromental assessment and historic erosion calculation of abandoned mine tailings from a semi-arid zone of northwestern Mexico: Insights from geochemistry and unmanned aerial vehicles. *Environ. Sci. Pollut. Res.* **2019**, *26*, 26203–26215. [CrossRef]